2019 International Conference on Robotics and Automation (ICRA)
Palais des congres de Montreal, Montreal, Canada, May 20-24, 2019

# Lift Your Leg: Mechanics of Running Through Fluids

Ryan Alicea*, Kyle Ladyko*, and Jonathan Clark*

***Abstract*— In order for legged robotic platforms to become adept enough to operate in unstructured, outdoor environments it is critical that they have the ability to adapt to a variety of terrains. One class of terrains to consider are regions of shallow, dense fluids, such as a beach-head, stream banks, snow or mud. This work examines the behavior of a simulated SLIP runner operating in such a viscous medium. Simulation results show that intelligently retracting the leg during flight can have a profound effect on the maximum achievable velocity of the runner, the stability of the resulting gait, and the cost of transport of the runner. Results also show that *trudging* gaits, in which the leg is positioned behind the center of mass, can be favorable in certain situations in terms of energy consumption and forward velocity.**

## I. INTRODUCTION

Contemporary legged robotics research is making progress towards developing machines which are able to mimic, or even improve upon, the natural and dynamic motion strategies observable in biology. One of the principle obstacles in the way of achieving this goal is the diversity of natural environments.

This work focuses on a singular terrain archetype that has been neglected in the contemporary body of work: terrain which can be described by a rigid ground layer covered by a layer of some viscous continuum of an arbitrary depth, be it water, snow, mud, or tall grass.

A large body of work has been completed deriving proper control strategies for high speed legged operation in controlled, laboratory environments. The Spring-Loaded Inverted Pendulum model (SLIP)[1], has become a staple of this area of research. This generalized model has shown a high degree of similarity to the dynamics of many legged animals and an applicability to the design and control of high-speed runners [2], [3], [4].

In the natural world, however, the properties of a terrain can vary widely. The physical geometry of natural environments is often rough, uneven, and irregular with a wide variance in terramechanics. General robot control strategies have been designed for SLIP-like runners to handle the geometric aspects of the problem including leg touch down control [5], Adaptive Energy Removal [6], and swing-leg retraction protocols [7]. Others have explored the dynamics of runners and legged robots on deformable terrain [8], [9]. However, there has been noticeable vacancy in the contemporary body of work addressing the issues of moving through littoral regions or other environments, where a portion of the leg (or the entire leg) is submersed. While some robots can traverse through shallow water, sand, snow, or other viscous mediums[10], [11], [12] they do not have the appropriate degrees of control to respond to the fluid-interaction mechanics intelligently.

*FAMU/FSU College of Engineering, Tallahassee, FL 32310
Center for Intelligent Systems Control and Robotics
Scansorial and Terrestrial Robotics and Integrated Design Lab
(rla11h, kcl14b)@my.fsu.edu, jeclark@fsu.edu

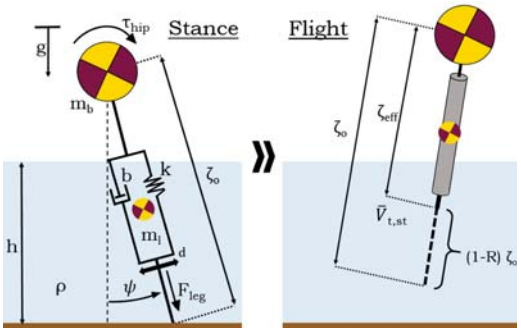


Fig. 1. Modified dynamic model of the SLIP template. The traditional SLIP model is augmented with (1) cylindrical leg having a distributed mass $m_l$, (2) fluid properties depth, $h$ and density, $\rho$, (3) a hip actuator providing a torque, $\tau_{hip}$, and a leg actuator providing a force, $F_{leg}$.

In this paper, we present a generalized model of running across a terrain covered in a viscous, fluid-like boundary layer. The modeling methods presented here are sufficiently general that they could be applied to many different types of legged robotic platforms.

In Section II we introduce the SLIP-Drag model which is designed to capture the large-scale fluid interactions between the runner and the environment. Section III describes the high-level simulation strategy used to obtain information about the model. In Section IV we examine how gait parameters impact the model while in the presence of varying amounts of fluid. The implications of these results are discussed in Section V. Section VI concludes the study and articulates the direction this work will go in the future.

## II. MODELING

### A. Dynamic Model

The model used in this research is derived from a classical, non-conservative, sagittal plane SLIP template. The primary modification to the runner itself is the addition of a cylindrical leg of uniform mass.

Shown in Fig. 1, the model is represented by a point mass, $m_b$, supported by a leg with stiffness, $k$, linear viscous damping properties, $b$, and a cylindrical geometry with diameter, $d$. During stance, the foot's position is invariant with no slippage occurring and acts as a fixed point about which the body and leg rotate. The center of mass of the

978-1-5386-6027-0/19/$31.00 ©2019 IEEE

cylindrical leg is assumed to be located at the midpoint of the leg at all times, $t$, during stance and flight.

The fluid is defined as a region with some height, $h$, and some density, $\rho$. The viscous forces of the fluid acting on the leg are generated through the combined effect of the forward velocity of the body as well as the rotational velocity of the leg about the center of mass of the body. Because the body of the runner is represented as a point mass, there is no fluid drag imposed on the main body of the runner as it moves through the fluid. It is important to note that small scale and high-frequency fluid interactions such as wakes and eddies are ignored. All buoyant forces are also ignored in these simulations.

In order to simplify the calculation of drag force acting on the submerged portion of the leg, a triangular tangential velocity profile acting on the leg is considered, as shown in Fig. 2a. The drag force is modeled as directly proportional to the velocity at any given point on the leg. With a velocity profile of this geometry, fluid-based drag forces can be treated as a distributed loading on the leg with the center of pressure located at the point of the leg moving at $\frac{2}{3}$ of the maximum tangential velocity. During flight, the average fluid interaction point is still treated at $\frac{2}{3}$ the maximum tangential velocity, shown in Fig. 2b, but the tangential velocity is now coupled with the velocity components contributed by the translational velocity of the system.

For the purpose of these simulations, the cylindrical leg's coefficient of drag, $C_D$, is approximated to be 1.0, a value extrapolated from research done on cylinders at similar Reynold's numbers that were varied in inclination angle [13].

Retraction of the leg occurs instantaneously after liftoff and is defined using a retraction factor, $R$. The retraction factor represents the fraction of the leg length which remains extended throughout the flight phase, shown in Fig.1b. Therefore, a retraction factor of 1 would indicate that the leg remains fully extended during flight. The minimum allowable retraction factors used in these simulations was set to 0.4 (or $60\%$ retracted), mimicking the range of motion of a Minitaur leg, discussed in Section II-C.

### B. Equations of Motion

For the purpose of this paper, one stride cycle is treated as the apex of one flight phase to the next. Each stride's trajectory is dictated by two sets of equations of motion derived using Lagrange's equations. Both sets of equations can be modeled in the same form:

$$\mathbf{M}(t)\ddot{\mathbf{q}}(t) = \mathbf{A}(t) + \mathbf{B}(t) + \mathbf{R}(t)\mathbf{F}(t) \tag{1}$$

where $\mathbf{q}(t)$ represents the state of the model, $\mathbf{M}$(t) composes the mass and inertia coefficients, $\mathbf{A}(t)$ is the actuation forces and torques, $\mathbf{B}(t)$ is the nonlinear terms derived from the Lagrangian, $\mathbf{R}(t)$ is the transformation of fluid forces to linear forces and torques, and $\mathbf{F}(t)$ represents the fluid drag forces on the model.

*1) Stance:* During the stance phase both the hip and leg are actuated as the center of mass rotates about the ground contact point, the matrices can be formed using the following relationships:

$$\mathbf{M}(t) = \begin{bmatrix} m_b + \frac{m_l}{4} & 0 \\ 0 & m_b\zeta^2 + \frac{m_l\zeta^2}{4} \end{bmatrix}, \quad \mathbf{q}(t) = \begin{bmatrix} \zeta \\ \psi \end{bmatrix}, \quad \mathbf{A}(t) = \begin{bmatrix} F_{act} \\ \tau_{hip} \end{bmatrix},$$

$$\mathbf{B}(t) = \begin{bmatrix} \zeta\dot{\psi}(m_b + \frac{m_l}{4}) - g\cos\psi(m_b + \frac{m_l}{2}) - b\dot{\zeta} - k(\zeta - \zeta_o) \\ g\zeta\sin\psi(m_b + \frac{m_l}{2}) - \zeta\dot{\zeta}\dot{\psi}(2m_b + \frac{m_l}{2}) \end{bmatrix},$$

$$\mathbf{R}(t) = \begin{bmatrix} 0 & 0 \\ 0 & \bar{\zeta} \end{bmatrix}, \quad \mathbf{F}(t) = \frac{C_D\rho A_s}{2}\begin{bmatrix} 0 \\ \bar{V}_{t,st}^2 \end{bmatrix}$$

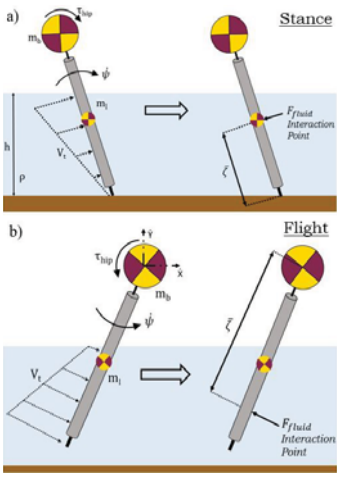


Fig. 2. During stance (a), the tangential velocity profile, $V_t$, is relative solely to the speed of rotation about the foot. The fluid interaction point, $\bar{\zeta}$, is taken as the location of the center of pressure of the distributed load of the viscous drag. During flight (b), the tangential velocity profile on the leg is produced by the combined effect of the system's translational and rotational velocities.

where $\zeta_o$ and $\zeta$ represent the equilibrium leg length from foot to body and the length from foot to leg mass at time $t$ respectively. The terms $\psi$, $g$, $m_b$, $m_l$, $b$, and $k$ represent the angle of the leg with respect to vertical, gravitational acceleration, the mass of the body, the mass of the leg, the leg damping coefficient, and the leg stiffness coefficient, respectively. The terms $F_{act}$, $\tau_{hip}$, $\tau_{fluid}$, and $\bar{\zeta}$ represent the prismatic force applied by the leg actuator, the torque applied by the hip actuator, the torque experienced about the center of mass from fluid-leg interaction, and the distance from the average fluid interaction point to foot, respectively. The terms $C_D$, $\rho$, $A_s$, $\bar{\zeta}$, and $\bar{V}_{t,st}$ represent the drag force coefficient of a cylinder, the fluid density, the surface of the cylinder interacting with fluid, the distance from the foot to fluid interaction point, and the tangential velocity of the leg during stance at fluid interaction point respectively. It is important to note here that during stance phase, fluid forces are only acting tangentially to the rotation of the center of mass about the foot.

*2) Flight:* The series of equations regarding the flight phase follow the same general form as Equation 1, where the matrices are now represented as:

$$\mathbf{M}(t) = \begin{bmatrix} m_b + m_l & 0 & \frac{m_l\zeta_o}{2}\cos\psi \\ 0 & m_b + m_l & \frac{m_l\zeta_o}{2}\sin\psi \\ \frac{m_l\zeta}{2}\cos\psi & \frac{m_l\zeta_o}{2}\sin\psi & \frac{5m\zeta_o{}^2}{6} \end{bmatrix}, \quad \mathbf{q}(t) = \begin{bmatrix} x \\ y \\ \psi \end{bmatrix},$$

$$\mathbf{A}(t) = \begin{bmatrix} 0 \\ 0 \\ \tau_{hip} \end{bmatrix}, \quad \mathbf{B}(t) = \begin{bmatrix} \frac{m_l \zeta_o \dot{\psi}^2}{2} \sin\psi \\ \frac{-m_l \zeta_o \dot{\psi}^2}{2} \cos\psi - m_b g \\ \frac{-m_l \zeta_o \dot{\psi}}{2} \sin\psi \end{bmatrix},$$

$$\mathbf{R}(t) = \begin{bmatrix} \cos\psi & 0 & 0 \\ 0 & \sin\psi & 0 \\ 0 & 0 & \bar{\zeta} \end{bmatrix}, \quad \mathbf{F}(t) = \frac{C_D \rho A_s}{2} \begin{bmatrix} \bar{V}_x^2 \\ \bar{V}_y^2 \\ \bar{V}_{t,fl}^2 \end{bmatrix}.$$

$\bar{\zeta}$ now denotes the length from body mass to fluid interaction point. $\bar{V}_x$, $\bar{V}_y$, and $\bar{V}_{t,fl}$ represents the velocity at the fluid interaction point with respect to the x, y, and tangential direction respectively.

Because the apex height of the body and leg angle change during flight, $\bar{\zeta}$ and $A_s$ are both functions of time, and receive different treatment during stance and flight phases. During flight phase $\bar{\zeta}$ is treated as the distance from the mean fluid interaction point to body mass, and is determined by the following:

$$\bar{\zeta}(t) = \begin{cases} \zeta_o - \frac{1}{3}\left(\frac{h - y_{foot}}{\cos\psi}\right) & \text{if y} \geq h, y_{foot} \leq h \\ \frac{2}{3}\zeta_o & \text{if y} < h, y_{foot} < h \\ 0 & \text{otherwise} \end{cases} \quad (2)$$

where $y_{foot}$ is the position of the foot in the Cartesian frame and $h$ is the height of fluid measured from ground. $\bar{\zeta}$ is the distance from mean fluid interaction point to foot, shown by:

$$\bar{\zeta}(t) = \frac{2}{3} \begin{cases} \frac{h}{\cos\psi} & \text{if y} \geq h \\ \zeta_o & \text{if y} < h \end{cases} \quad (3)$$

Transition from stance to flight occurs when the vertical ground reaction force of the leg becomes zero.

$$\cos\psi\big(k(\zeta - \zeta_o) - b\dot{\zeta}\big) + \frac{\tau_{hip}}{\zeta} \sin\psi = 0$$

Actuation at the hip occurs for the entire duration of one stride. During stance, it is used to regulate the forward velocity, while during flight is serves to achieve the desired touch down angle, which is discussed in Section II-C. Prismatic actuation of the leg occurs during stance phase after the leg has reached maximum compression. Simple motor models were used for both the hip and leg actuators but were implemented using specifications for real actuators (Section II-C). These models allowed the actuation methods to be limited by the appropriate speed-torque curve.

TABLE I

RANGE OF THE PARAMETER SPACE

| Parameters | Notation | Minimum | Maximum | Units |
|---|---|---|---|---|
| Desired Velocity[a] | $\dot{x}$ | 0 | 3 | $\frac{m}{s}$ |
| Touchdown Angle | $\psi$ | $\frac{-\pi}{12}$ | $\frac{\pi}{9}$ | rad |
| Retraction Factor[b] | $R$ | 1 | 0.4 | - |
| Fluid Depth[c] | $D$ | 0 | 1.30 | - |
| Fluid Density | $\rho$ | 1000 | 25000 | $\frac{kg}{m^3}$ |

[a]Resultant behavior of the model often differs from control velocity
[b]Fraction of the leg which remains extended during flight
[c]Normalized to rest length of the leg

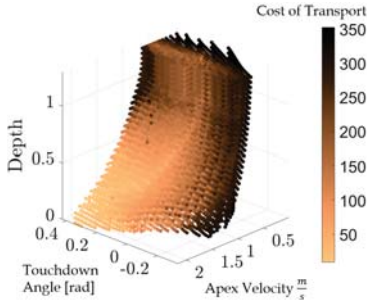


Fig. 3. Three-dimensional cross section of parameter sweep results, taken at $\rho = 1000\frac{kg}{m^3}$ with $R = 1$ (no retraction). Each data point represents the results of a single simulation (failed or higher-period gaits are not depicted). From this, qualitative behavior of the model can be inferred. It is clear that fluid has a large impact on the achievable velocity of the model and that the most efficient forms of locomotion occur in very shallow fluids for straight-leg running.

### C. Physical Parameters and Control

Finally, to simulate fluid interactions more accurately, physical parameters of the model were selected to mimic a single leg of the Minitaur quadruped robot which is developed by Ghost Robotics. A simple motor model of the DYS U8 Pro $100Kv$ in a direct-drive configuration was included.

TABLE II

PHYSICAL MODEL PARAMETERS AND CONSTANTS

| Parameters | Notation | Value | Units |
|---|---|---|---|
| Body Mass | $m_b$ | 1.6 | kg |
| Leg Mass | $m_l$ | 0.28 | kg |
| Leg Rest Length | $\zeta_o$ | 0.20 | m |
| Leg Stiffness | $k$ | 1500 | $\frac{N}{m}$ |
| Leg Damping Coefficient | $b$ | 0.0914 | $\frac{Ns}{m}$ |
| Motor No-Load Speed | $\omega_{nl}$ | 157[a] | $\frac{rad}{s}$ |
| Motor Stall Torque | $\tau_{stall}$ | 5.9[a] | Nm |
| Motor Internal Resistance | $R_m$ | 0.2542 | $\Omega$ |
| Leg Motor Crank Arm | $r$ | 0.00875 | m |
| Leg Diameter | $d$ | 0.015 | m |
| Coefficient of Drag | $C_D$ | 1[b] | - |
| Gravitational acceleration | $g$ | 9.81 | $\frac{m}{s^2}$ |

There are two low-level controllers at work in the simulation of the model. The first handles the positioning of the leg during flight using a PD control scheme, the second maintains forward velocity during stance. Leg actuation operates using a very simple control method: a voltage is applied to the motor when the leg reaches maximum compression ($\dot{\zeta} \geq 0$). These control mechanisms are shown in the following equations respectively:

$$\tau_{hip} = K_p\big(\psi_{des} - \psi\big) + K_d\big(\dot{\psi}_{des} - \dot{\psi}\big) \quad (4)$$

$$\tau_{hip} = K_p\big(\dot{x}_{des} - \dot{x}\big) \quad (5)$$

$$F_{leg} = \begin{cases} \frac{\omega_{nl} - \frac{\dot{\zeta}}{r}}{R_m} & \text{if } \dot{\zeta} \geq 0 \\ 0 & \text{if } \dot{\zeta} < 0 \end{cases} \quad (6)$$

[a]Parameters valid for both hip and leg actuators
[b]Parameter obtained from external research[13]

These controllers have been re-purposed from the foundational works of Raibert [14][15] and were selected in an effort to keep the model as generalizable as possible. Gains for these controllers were selected by passing a large number of simulations on fluid-free terrain into a Particle Swarm Optimizer [16] with a cost function derived from the Mean-Squared-Error of the forward velocity, hop height, and leg position of two consecutive strides at apex. Each simulation was initiated at the stable, steady-state behavior of the model for that particular set of gait parameters. The stability criteria used in this work requires that $|\lambda_{max}| < 1$ where $\lambda$, are the eigenvalues of the linearized return map. Thus, any failed or unstable gaits are discarded and do not appear in the final data. For simplicity of analysis, only period-one gaits are considered in this work, though many higher-period gaits exist within the parameter space. It is important to note that the instantaneous retraction and extension of the leg is not energetically free. The energy cost associated with retracting and extending the leg was computed from the current recorded during a series of extensions and retractions done by a Minitaur leg and estimated to be approximately $2.25J$ per percent of rest length retracted or extended.

## III. Simulation Procedure

In order to explore the nature of the runner's interaction with a fluid, a parameter sweep was performed. The five-dimensional space explored consisted of the leg touchdown angle, $\psi$, the desired forward velocity, $\dot{x}$, the retraction factor of the leg, $R$, the normalized depth of the fluid, $D$, and the density of the fluid, $\rho$. For each simulation, cost of transport was calculated according to its definition $COT = \frac{E}{mgd}$,

where $E$ is the energy expended by the model during the trial, $m$ is the total mass of the model, $d$ represents the total distance traveled by the model, and $g$ is the gravitational constant. The range of values examined is shown in Table I. All simulations were constructed in the Matlab 2018 environment and solved using the Runge-Kutta analysis method, ode45.

## IV. Results

### A. Fluid Depth and Viscosity

Fig. 3 depicts a single three-dimensional cross-section of the results of the parameter sweep. It is clear that the presence of a fluid has a significant impact on the resultant behavior of the runner. In order to simplify the analysis of the parameter space, additional two-dimensional cross-sections are taken at different touchdown angles. Fig. 4 shows a number of these cross-sections and illustrates the effects of fluid viscosity and depth on the resulting behavior of the model. As shown in Fig. 4a, a runner operating in a relatively thin fluid of $\rho = 1000\frac{kg}{m^3}$ that is not retracting its leg will begin to experience a reduction in maximum apex velocity when $D > 0.1L$. Operation at any depth greater than this reduces the achievable forward velocity. As the viscosity of the fluid increases, this upper limit of operation decreases such that it approaches $D = 0L$. Within high-drag environments (Fig. 4c) and without any margin of leg retraction, the runner is unable to operate at $D > 1.1L$. This range of operation is further reduced to $D < 0.55L$ as density increases to $\rho \geq 25000\frac{kg}{m^3}$ (Fig. 4d).

The rate of velocity falloff increases dramatically when comparing a relatively inviscid fluid (Fig. 4a) with running behavior in more dense fluid (Fig. 4b). From this relationship it can be inferred that the rate of velocity falloff with respect to depth is a function of the fluid viscosity. However, this rate appears to stabilize as the depth of the fluid approaches and exceeds the resting leg length ($D \geq 1L$). It appears that when a certain depth is reached, the maximum velocity becomes a function of both the actuator limits and fluid properties.

### B. Leg Retraction

As shown in Figs. 4(a-d), retracting the leg by 60% allows the runner to operate at maximum velocity in most drag-inducing environments while $D < 0.6L$. An identical runner without leg retraction would not be able to move at that speed in a relatively inviscid fluid with the properties of water ($\rho = 1000\frac{kg}{m^3}$), for any depths exceeding $D = 0.1L$. Within such a relatively inviscid fluid, at a depth exceeding the resting leg length ($D = 1.3L$), a runner operating with a full leg retraction ($60\%$ or $R = 0.4$) is able to achieve 171% greater velocities than a straight-leg runner ($1.73\frac{m}{s}$ vs. $1.014\frac{m}{s}$). The fully retracted runner maintained a $COT = 60$ while the straight-leg runner maintained a $COT = 204$, thus not only moving faster in deeper fluid but doing so while reducing its cost of transport by more than a factor of three. When operating in a significantly more viscous environment, as in Figs. 4(b-c), a runner taking advantage of leg retraction is able to maintain maximum velocity while $D < 0.6L$.

As shown in Fig 4(a-c), the critical depth at which velocity reduction begins to occur maintains very near to a 1:1 relationship with the amount of leg retracted, or more formally:

$$D_{crit} \approx (1 - R) \tag{7}$$

### C. Negative Touchdown Angles

As effective as retraction of the leg appears to be at both maintaining velocity and reducing overall cost of transport, another type of behavior emerges which has useful properties for operation in regions of deep fluid. In Fig. 5, it can be seen that there are circumstances in which negative touchdown angles, when the foot touches down *behind* the center of mass, can be more efficient. The benefits of this type of behavior only begin to appear in deep fluid ($D > 0.6L$) and occur regardless of the amount of specified leg retraction. As the highlighted points indicate, under certain conditions, it is possible to operate in a deeper fluid at a lower cost by maintaining a negative angle of touchdown. This type of gait appears to be most efficient at low desired velocities.

Fig. 6 depicts an additional example of a high-efficiency region of low touchdown angles which develops as $D \geq 0.76L$ within an otherwise low-efficiency domain of operation. As depth increases, it can be observed that this high-efficiency region migrates from very low angles at touchdown to steeper, but still negative, angles while maintaining the same apex velocity.

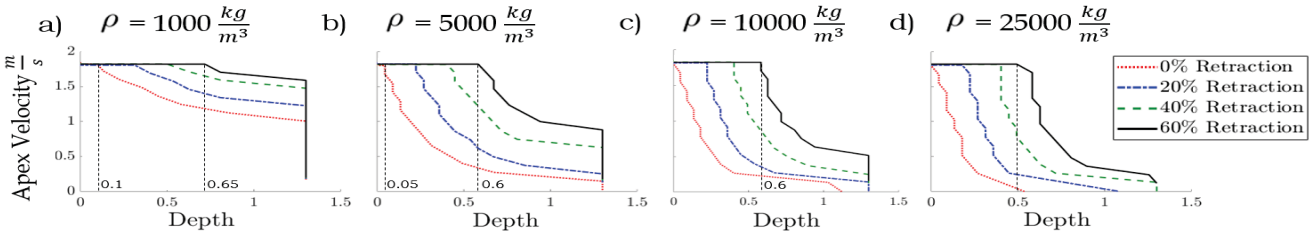


Fig. 4. Comparison of the maximum apex velocities versus the normalized depth of a runner utilizing different amounts of leg retraction. Two-dimensional cross-sections were taken at constant touch down angle, $\psi = 0.07rad$. Leg retraction has a demonstrable effect on the viability of the gait of a runner operating in a high-drag environment. Vertical dashed lines indicate the depth at which the runner becomes unable to maintain forward velocity. The area under each curve represents the region of stable operation. It can be observed that the depth threshold at which the maximum velocity of the model begins to deteriorate maintains a nearly 1:1 ratio with the amount of leg retracted.

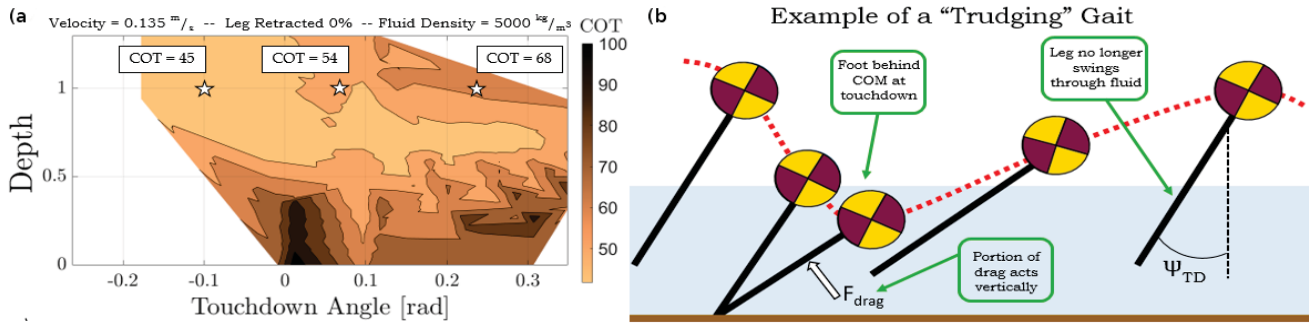


Fig. 5. (a) Cross-section, taken with respect to velocity, fluid density and retraction factor, highlighting an instance where a trudging gait can be desirable. The points marked with stars are used to illustrate the relatively low cost of transport for negative touch down angles in deeper fluid. Trudge-style gaits also appear to only become efficient when the desired velocity is relatively low. (b) An illustration of the model behavior during a trudge gait. Even before touchdown, a fraction of the fluid drag is acting vertically, slowing the model as it descends and helping to support it during stance, reducing the load seen by the hip actuator. Throughout takeoff and flight, fluid drag acting on the leg is significantly reduced due to the more streamlined position and the lack of a need to swing the leg through the fluid during flight.

## V. Discussion

### A. Fluids Can Be a Severe Impediment to Motion

Any layer of a viscous medium can become an impediment to motion. For example, as in the cases of Fig. 4b, even small amounts of a fluid reduce the velocity of the system. In many cases when the fluid viscosity is high, as in Figs. 4(c-d), the runner is unable to operate at all when the depth of the fluid exceeds a certain threshold.

It should be noted that though the runner is *able* to operate at these boundaries does not mean that it is effective; the forward velocity of the model approaches $0\frac{m}{s}$ as the depth approaches these boundaries. The rate of velocity depreciation with depth grows with the density of the fluid. It seems apparent that this rate could be described as some function of the fluid viscosity (Fig. 4).

It may seem a bit impractical to consider fluids with a density of $10000\frac{kg}{m^3}$ or $25000\frac{kg}{m^3}$. It is important to consider that the behavior of the runner does not actually depend on fluid density but rather the drag forces experienced by the runner, regardless of their origin. The geometry of the model used in these simulations is overly simplistic. A runner with more intricate leg architecture, a larger leg diameter, or any protrusions, such as a foot, may be perfectly capable of experiencing large drag forces comparable to that of a very dense fluid interacting with a cylinder. It is for these reasons that it may be of some importance to consider the model behavior under these extreme circumstances.

### B. Leg Retraction Augments Performance

Leg retraction is an effective mechanism for a runner to reduce its level of interaction with the fluid and allows the runner to improve its performance in high-drag environments. The benefits of this include:

- Increase in Traversable Depth
- Higher Speeds at Depth
- Increased Efficiency
- Improved Stability

*1) Increase in Traversable Depth:* Runners which do not sufficiently lift their leg will often become perturbed by the fluid and fail as they attempt to reposition their leg during flight. As the viscosity becomes greater, this type of failure becomes increasingly common. As illustrated in Fig. 4(a-d), increasing leg retraction has a strong and measurable impact on the depths within which it is able to operate, as presented in Section IV-A. A runner retracting its leg is able to mitigate this effect substantially, allowing for operation at greater depths.

*2) Increased Velocity:* Even when a runner is completely submerged in a fluid $(D \geq 1L)$ runners which take advantage of leg retraction have a higher apex velocity and a lower cost of transport than those that do not. Retraction of the leg

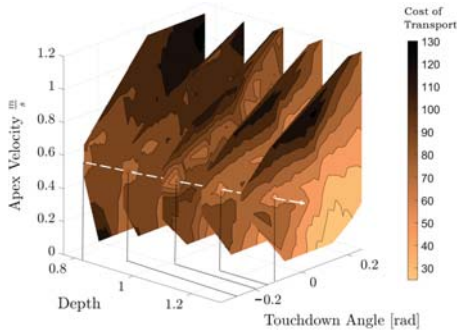


Fig. 6. Two-dimensional cross sections taken at five different normalized depths in an environment which provided significant resistance to the locomotion of the runner ($\rho = 25000$). Each cross section is taken at a depth which exceeds the retraction capability of the model. It can be observed that under these conditions, there exists a consistent and narrow low-cost region of operation for sharp, negative touchdown angles ($\psi < 0$). As the depth increases further, this low-cost region shifts towards more positive angles at touchdown. Perturbations of the model touchdown angle and velocity about this region of operation do not result in significant *observable* differences in behavior though the cost of transport may be reduced by nearly a factor of two.

condenses the amount of exposed surface area seen by the free stream velocity of the fluid. Additionally, leg retraction brings the center of mass of the leg and the fluid interaction point closer to the center of mass of the model, reducing the moment arm of the fluid force on the runner.

*3) Increased Stability:* When running at high speed, fluid effects become an impediment even when only a small portion of the leg interacts with the medium during flight. In many instances, a runner that is not lifting its leg adequately will become perturbed by this fluid interaction such that it trips while attempting to reposition its leg. As the viscosity of the fluid increases, the actuators, unable to overcome the resistance of the high-drag environment, fail to effectively reposition the leg to the touchdown position.

*4) Increased Efficiency:* In all instances where $D > 0.1L$, retracting the leg allowed the runner to achieve a lower cost of transport when operating in the same environment as a straight-leg runner. As the leg is retracted, the drag forces experienced by the leg are reduced thus lowering the control effort required by the hip actuator to move the leg through the fluid, resulting in a lower cost of transport for the runner.

*5) Maximizing Performance:* Leg retraction augments the performance of the runner in all environments in which fluid is present, but it is important not to over-retract. A needlessly high leg retraction results in unnecessary energy expenditure and a resultant increase in $COT$. The relationship presented in Eqn. 7 identifies an optimal region of leg retraction.

### C. Negative Touchdown Angles Can Reduce Cost

For a classical SLIP runner, touchdown angle is typically positive. However, in a high-drag environment, it appears that touching down with the foot *behind* the center of mass can be more efficient in certain cases (Figs. 5, 6). As the depth of the fluid exceeds the length of the leg during flight, high-efficiency regions develop for gaits with negative touchdown angles. These "trudging" gaits can allow for a low $COT$ in nearly all deep fluid conditions regardless of the amount of leg retraction or fluid viscosity.

Similarly to leg retraction, holding the leg behind the center of mass during flight can serve as another mechanism to reduce the exposed surface area of the leg to the effective free stream velocity of the fluid, thus reducing the drag acting on the runner. In addition, during stance phase, the drag forces only act tangentially to the rotation of the leg, as described in Section II. If the leg is placed behind the center of mass at touchdown, a percentage of the drag force from the fluid serves as a support for the model, resulting in a reduction of the torques required from the motors in order to keep the model upright (Fig. 5b).

## VI. Conclusions and Future Work

This work presents a novel modification to the SLIP model of running that is able to capture the fluid interaction mechanics while running through a high-drag environment. Simulation results suggest that retracting the leg is a cost-efficient technique which can improve the overall performance of the runner with respect to traversability, maximum velocity, and cost of transport. Through leg retraction, the effective surface area of the leg is reduced and in turn reduces the effort needed by actuators to move the leg through the fluid. This increases the traversable fluid depth, achievable velocities, stability, and efficiency when running through a viscous medium. Although leg retraction is a powerful tool, it is important to note that over-retracting when traversing shallow fluids can result in an unnecessary increase in cost of transport. We have also shown that negative touchdown angles have a similar utility when operating within a medium which is too deep to clear during flight, as the drag forces experienced can actually aid the runner in stability and efficiency.

Moving forward, we are developing a physical test environment is conjunction with the Army Research Laboratory (ARL) in order to experimentally validate the results presented in this work. More work can also be done to refine this model, including considering cohesive properties of the medium, higher-order wake behavior, and changes in drag coefficient while inclined. This may improve its relevance to a real-world environment such as snow, mud or deformable vegetation.

These types of fluid-like terrains are largely intractable to current legged robotic platforms. A SLIP-like runner that explicitly uses a fluid drag model as apart of its gait development, as outlined in this paper, should be able to operate in these types of terrain much more efficiently than the current state-of-the-art.

## Acknowledgements

This work was supported by the collaborative participation in the Robotics Consortium sponsored by the U.S. Army Research Laboratory under the Collaborative Technology Alliance Program, Cooperative Agreement DAAD 19-01-2-0012. The U.S. Government is authorized to reproduce and distribute reprints for Government purposes not withstanding any copyright notation thereon.

## REFERENCES


[1] R. Blickhan, "The spring-mass model for running and hopping," *Journal of biomechanics*, vol. 22, no. 11-12, pp. 1217–1227, 1989.

[2] R. M. Alexander, "A model of bipedal locomotion on compliant legs," *Phil. Trans. R. Soc. Lond. B*, vol. 338, no. 1284, pp. 189–198, 1992.

[3] C. Hubicki, A. Abate, P. Clary, S. Rezazadeh, M. Jones, A. Peekema, J. Van Why, R. Domres, A. Wu, W. Martin *et al.*, "Walking and running with passive compliance: Lessons from engineering a live demonstration of the atrias biped," *IEEE Robotics & Automation Magazine*, no. 99, pp. 1–1, 2018.

[4] A. V. Birn-Jeffery, C. M. Hubicki, Y. Blum, D. Renjewski, J. W. Hurst, and M. A. Daley, "Don't break a leg: running birds from quail to ostrich prioritise leg safety and economy on uneven terrain," *Journal of Experimental Biology*, vol. 217, no. 21, pp. 3786–3796, 2014.

[5] J. K. Hodgins and M. Raibert, "Adjusting step length for rough terrain locomotion," *IEEE Transactions on Robotics and Automation*, vol. 7, no. 3, pp. 289–298, 1991.

[6] B. Andrews, B. Miller, J. Schmitt, and J. E. Clark, "Running over unknown rough terrain with a one-legged planar robot," *Bioinspiration & biomimetics*, vol. 6, no. 2, p. 026009, 2011.

[7] A. Seyfarth, H. Geyer, and H. Herr, "Swing-leg retraction: a simple control model for stable running," *Journal of Experimental Biology*, vol. 206, no. 15, pp. 2547–2555, 2003.

[8] C. Li, T. Zhang, and D. I. Goldman, "A terradynamics of legged locomotion on granular media," *Science*, vol. 339, no. 6126, pp. 1408–1412, 2013.

[9] C. M. Hubicki, J. J. Aguilar, D. I. Goldman, and A. D. Ames, "Tractable terrain-aware motion planning on granular media: An impulsive jumping study," in *Intelligent Robots and Systems (IROS), 2016 IEEE/RSJ International Conference on*. IEEE, 2016, pp. 3887–3892.

[10] A. Crespi, K. Karakasiliotis, A. Guignard, and A. J. Ijspeert, "Salamandra robotica ii: an amphibious robot to study salamander-like swimming and walking gaits," *IEEE Transactions on Robotics*, vol. 29, no. 2, pp. 308–320, 2013.

[11] G. Dudek, M. Jenkin, C. Prahacs, A. Hogue, J. Sattar, P. Giguere, A. German, H. Liu, S. Saunderson, A. Ripsman *et al.*, "A visually guided swimming robot," in *Intelligent Robots and Systems, 2005.(IROS 2005). 2005 IEEE/RSJ International Conference on*. IEEE, 2005, pp. 3604–3609.

[12] A. S. Boxerbaum, P. Werk, R. D. Quinn, and R. Vaidyanathan, "Design of an autonomous amphibious robot for surf zone operation: Part i mechanical design for multi-mode mobility," in *Proceedings, 2005 IEEE/ASME International Conference on Advanced Intelligent Mechatronics.* IEEE, 2005, pp. 1459–1464.

[13] A. Vakil and S. I. Green, "Drag and lift coefficients of inclined finite circular cylinders at moderate reynolds numbers," *Computers & Fluids*, vol. 38, no. 9, pp. 1771–1781, 2009.

[14] M. H. Raibert, H. B. Brown Jr, and M. Chepponis, "Experiments in balance with a 3d one-legged hopping machine," *The International Journal of Robotics Research*, vol. 3, no. 2, pp. 75–92, 1984.

[15] M. Raibert, M. Chepponis, and H. Brown, "Running on four legs as though they were one," *IEEE Journal on Robotics and Automation*, vol. 2, no. 2, pp. 70–82, 1986.

[16] I. C. Trelea, "The particle swarm optimization algorithm: convergence analysis and parameter selection," *Information processing letters*, vol. 85, no. 6, pp. 317–325, 2003.